# Different Head Group Dependence on The Lipid Thermodynamic Property of Myelin Basic Protein in the Lipid Monolayer

**Lei Zhang** ( 15229244102@163.com )
Xi'an Aeronautical University
**Ming Zhang**
Xi'an Aeronautical University
**Runguang Sun**
Shaanxi Normal University

**Research Article**

**Keywords:** MBP, Lipid monolayers, Isotherm, Virial coefficients, Atomic force microscopy

**Posted Date:** February 4th, 2021

**DOI:** https://doi.org/10.21203/rs.3.rs-154189/v1

# Different Head Group Dependence on the Lipid Thermodynamic Property of Myelin Basic Protein in the Lipid Monolayer

Lei Zhang[1*], Ming Zhang[1],Runguang Sun[2]

[1]Department of Experimental Teaching Center for Optoelectronic Science and Information Engineering, Xi'an Aeronautical University, Xi'an 710077, China

[2]School of Physics and Information Technology, Shaanxi Normal University, Xi'an 710062, China

15229244102@qq.com; https://orcid.org/0000-0002-8204-1927 (Lei Zhang)

## Abstract

The interaction between the role of 18.5 KDa myelin basic protein (MBP) isoform and phospholipids has been thought to maintain the stability and compactness of the myelin sheath structure. In this study, we describe the statistical thermodynamic theory of different concentrations' effects on MBP in the major myelin lipid (1-palmitoyl-2-oleoyl-sn-glycero-3-phosphocholine (POPC), 1-palmitoyl-2-oleoyl-sn-glycero-3-phosphoethanolamine (POPE)，and 1-palmitoyl-2-oleoyl-sn-glycero-3-phospho-L-serine (POPS)) monolayers at the air/subphase interface via Langmuir-Blodgett (LB) technique. A simple statistical mechanical theory is established that predicts the interaction between proteins and phosphate head groups at low surface pressures and the second virial coefficient dependences for the PC, PE, and PS head groups are illustrated. In addition, the surface pressure(π)-mean molecular area(mma) curves were also analyzed using two-dimensional virial equation of state (2D-VES). The positively charged showed that MBP may integrate into different lipid monolayers via hydrophobic and electrostatic interactions, which was found to be consistent with AFM observations of domain and aggregate structures as well as with changes in the surface morphology induced by MBP. These analyses pertaining to membrane structure will provide better insight into membrane modeling systems, especially the interaction between membrane molecules.

**Keywords:** MBP · Lipid monolayers · Isotherm · Virial coefficients · Atomic force microscopy

## Introduction

Myelin basic protein (MBP) is an important component of myelin. The severity and extent of nerve injury as well as its outcome and prognosis of the disease require the detection of MBP concentration in serum and cerebrospinal fluid (CSF). The central nervous system (CNS) and peripheral nervous system (PNS) compacted myelin proteins are MBP, which accounts for about 30% of the total myelin sheath [1,2]. Specifically, 18.5 KDa MBP is the main protein in the mature myelin of the CNS and is the most conserved protein in the MBP family during evolution. It is reported that

the 18.5 KDa MBP of vertebrates contains 170 amino acid residues that play a key role in the structure and function of the protein [3,4]. It interacts with the phospholipids of different heads of the myelin membrane, promoting the fusion of oligodendrocytes and forming the main dense line of the multi-layer membrane structure [5,6]. For good measure, the interaction between MBP and myelin membrane phospholipids may be closely combined, which confers stability to the myelin structure and function. Moreover, nerve conduction insulation is improved along with conduction speeds, playing a very important role in myelin formation as well as brain differentiation and maturation [7-9].

In our previous studies [10-12], we have investigated the adsorption of MBP at the free air/subphase interface and onto different monolayers at the interface. The results showed that the surface phenomena are closely related to the concentration of protein, surface pressure, subphase and so forth. Additionally, we found that the adsorption of MBP into the various phospholipids was necessary due to the electrostatic and hydrophobic interactions between the penetrating MBP and the negatively charged head and hydrocarbon chains of the phospholipids. However, other studies have shown that the lipid monolayers possessed a lipid composition of myelin, such as dipalmitoylphosphatidylcholines (DPPC) [13], dipalmitoylphosphatidylserine (DPPS) [14], phosphatidylglycerol (PG) [15], and phosphatidicacid (PA) [16]. Among them, the myelin lipids (neutral POPC and POPE as well as anionic POPS) had interesting thermodynamic properties in the two-dimensional interfacial phase. POPC, POPE, and POPS have the same hydrophobic tail chain and contain 18 carbon atoms in each fatty acyl chain, but their hydrophilic headgroups are different [17]. The chemical structures of MBP, POPC, POPE, and POPS are shown in Fig.1.

This investigation does not study the transverse structure of myelin such as nerve impulse propagation, conductivity, and membrane order perturbation; it focuses on the lateral organization adopted by the proteins and myelin lipids when the monolayer is formed at the air/subphase interface. Essentially, the influence of MBP on the dynamics and structure of myelin membranes model was explored using Langmuir-Blodgett (LB) technology and an atomic force microscope (AFM). AFM is a powerful tool for the analysis of lipid-protein interactions and the formation of microdomains. This study regarding the supramolecular structure of myelin is of biophysical significance and medical value.

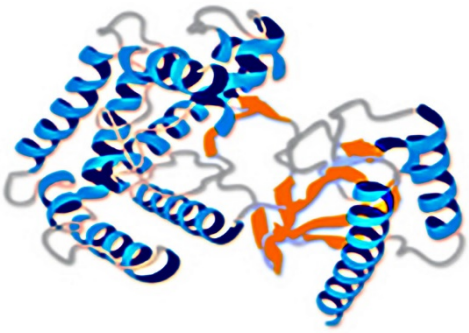

(a) MBP

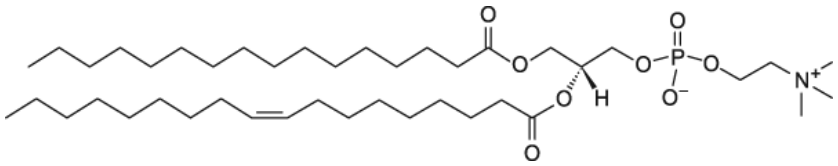

(b) POPC (zwitterionic)

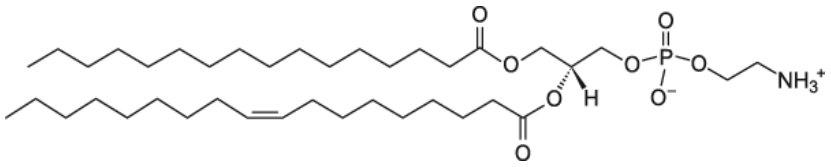

(c) POPE (zwitterionic)

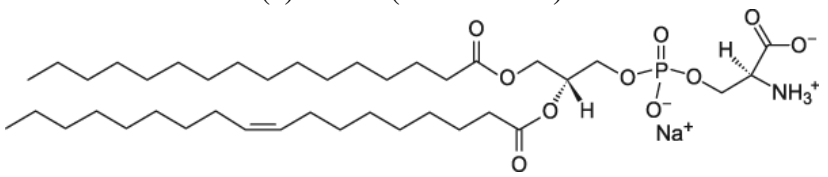

(d) POPS (anionic)

**Fig.1** The chemical structure of (a) MBP, (b) POPC, (c) POPE, and (d) POPS

## Materials and methods

### Chemicals

The protein used in the experiments, MBP, was collected and extracted from the bovine brain and purified in a water-soluble solution according to the procedures described by Deibler et al. [18]. It was then dialyzed against pure Millipore water and used at a concentration of $1.0\times10^{-9}$ M. The buffer was 10 mM Tris-HCL, and the pH was adjusted to 7.2. 1-palmitoyl-2-oleoyl-glycero-3-phosphocholine (POPC, molecular weight 760.1 g/mol), 1-palmitoyl-2-oleoyl-sn-glycero-3-phosphoethanolamine (sodium salt) (POPE, molecular weight 718.0 g/mol), and 1-palmitoyl-2-oleoyl-sn-glycero-3-phospho-L-serine (sodium salt) (POPS, molecular weight 784.0 g/mol) of high a purity (at least 99%) were purchased from Avanti Polar Lipids, Inc. (Alabaster, AL, USA) and used without further purification. Working solutions of lipids (1mg/ml) were dissolved in chloroform/methanol 3:1 v/v

mixture. The water (with a resistivity higher than 18.2 MΩcm) used in the experiment was obtained from a Millipore purification system.

## Isotherms

Langmuir experiments were fabricated with a KSV Minitrough system (Helsinki, Finland) with an operational area of 273 $cm^2$. All experiments were performed using Tris-HCl as the subphase. The Tris-HCl buffer solutions were prepared by Tris (hydroxyethyl) amino-methane (concentration of 10 mM) and titrated with HCl solution to the desired pH value (pH = 7.2). Prior to each measurement, the LB trough and barriers were thoroughly washed and wiped with ethanol and triple distilled water several times. The appropriate amount of lipid solutions (30 μL) was spread with precision microvolume syringes onto the subphase containing the moderate MBP. The solvent was allowed to evaporate for 15 minutes until the surface pressure (π) was stabilized. Subsequently, the monolayer was compressed to obtain the surface pressure versus area (π-A) isotherms. The constant rate of barrier during compression was 10 mm/min at a fixed temperature of 22±1 ℃ via circulating water bath. Each run was repeated at least three times to obtain reproducible results.

## Langmuir-Blodgett (LB) transfer

Transfer of amphiphilic monolayers onto the mica substrate was achieved using the Langmuir-Blodgett technique. Prior to transferring, freshly cleaved mica was immersed into the Tris-HCl subphase. Then, the barriers were compressed up to the desired surface pressure of 10 mN/m. Following 15 minutes of stabilizing the monolayer, the mica sheet was removed from the subphase with a constant dipper rate of 20 mm/min to obtain the transfer ratio of 1.0 ± 0.1.

## Atomic force microscopy

The transferred amphiphilic monolayers were monitored using a SPM-9500-J3 Atomic Force Microscope (AFM, Shimadzu Corporation, Japan). The scans were performed in contact mode using a Micro V-shaped Cantilever (Olympus Optical Co. Ltd., Japan) with a spring constant = 0.06 N/m, length of 100 μm, and thickness of 400 nm. The scan rate was 1.0 Hz per line with a resolution of 512 pixels per line.

## Theoretical analysis

### Phase transitions

The viscoelastic properties of the different monolayers were determined by calculating surface compressibility modulus values ( $C_s^{-1}$ ) from the π-A curves as:

$$C_s^{-1} = -A\left(\frac{\partial \pi}{\partial A}\right) \quad (1)$$

where $A$ is the average molecular area at the indicated surface pressure and $\pi$ is the corresponding surface pressure. The higher the compression modulus value of $C_s^{-1}$, the lower the elasticity of the monolayer, or the more ordered the monolayers [19].

**Virial coefficients for different lipids and MBP interactions**

The π-A isotherms in the region starting from the isotherms to π = 10 mN/m were fitted into the following two-dimensional virial equation of state (2D-VES) [20]:

$$\frac{\pi A}{kT} = a + b\pi + c\pi^2 \quad (2)$$

where $a$ denotes the aggregation coefficient. If $a = 1$, there is no aggregation between molecules at a low surface pressure, however, when $a < 1$, aggregation occurs between molecules, and the lower the value of a, the higher the degree of aggregation. $b$ is the virial coefficient, where $b > 0$ and $b < 0$ characterize the repulsive and attractive properties of the intermolecular interaction, respectively.

## Results and discussion

### π-A isotherm measurements of Tris-HCl subphase containing 1nM MBP with POPC, POPE, and POPS monolayers

This experiment analyzed the behavior of MBP which was incorporated into myelin sheath membranes, consisting of three very important lipids: POPC, POPE, and POPS. The concentration of MBP in the subphase changed with 1 nM. From the π-A isotherms observed in Fig.2 at a wide range of surface pressures (0~50 mN/m), the addition of lipids of different head groups to the Tris-HCL subphase containing 1.0 nM MBP was found to produce higher values in mean molecular area as the concentration rose, indicating the existence of interactions between the MBP and phospholipids. Pure POPC isotherm embodied a liquid-expanded (LE) phase during compression under the present study's experimental conditions. The compression of the barriers to surface pressure above 40.6 mN/m (equivalent to A = 54.8 Å$^2$) generally led to the collapse of the film. These results aligned with those of previously reported isotherms [21, 22]. The mixed monolayer curve possessed an identical smooth shape and operated almost in parallel to each other (Fig.2a). POPE is different from POPC in that it exhibited a fluid liquid-expanded (LE) phase up to 36.0 mN/m, where a phase transition between two liquid-condensed entities (namely LC and LC′) occurred [23, 24]. The mixed monolayer, with $C_{MBP}$ = 1 nM, demonstrated a LC-LC′ phase transition but at π = 34.9 mN/m, along with a collapse in surface pressure ($\pi_c$) of 37.5 mN/m. This implies that MBP adsorbed onto the POPE monolayer to make the

monolayer closer, resulting in smaller values of phase transition and collapsing pressures (Fig.2b). In terms of POPS, the isotherm demonstrated a LE phase state of the monolayer. The collapse pressure of the isotherm appears at $\pi$ = 36.5 mN/m [25]. the isotherms with 1nM MBP show higher mma's than the isotherm of pure POPS. This outcome was probably due to the adsorption of MBP onto the monolayer.

Fig. 2 (inset) illustrates that the isotherm of POPC confers the highest elasticity moduli of 108.5 mN/m, followed by POPE and POPS at 94.6 mN/m and 59.5 mN/m. respectively. Furthermore, as seen in Fig.2, the pure POPC, POPE and POPS monolayers possessed greater values of $C_s^{-1}$ with compression, indicating that the adsorption of MBP enables the monolayer to become unstable and loose.

According to Fig.3, all mixed monolayers demonstrated an increased mean molecular area in all phases compared to the isotherm of pure lipids. In addition, the POPS-MBP mixed monolayer exhibited greater mma's change in % than that of the POPC-MBP and POPE-MBP monolayers. The results revealed that the monolayer stability of the three lipids with MBP ($C_{MBP}$ = 1.0 nM) mixtures increases in the order of POPS-MBP < POPC-MBP < POPE-MBP. The insertion of the MBP protein in different lipid monolayers at a pressure of 10 mN/m suggests the existence of hydrophobic and electrostatic interactive behaviors. Table 1 summarizes the mean molecular area (Å$^2$) at lift-off, at a $\pi$ of 10 mN/m and at collapse, along with the percentage change with MBP = 1 nM in the POPC, POPE, and POPS monolayers.

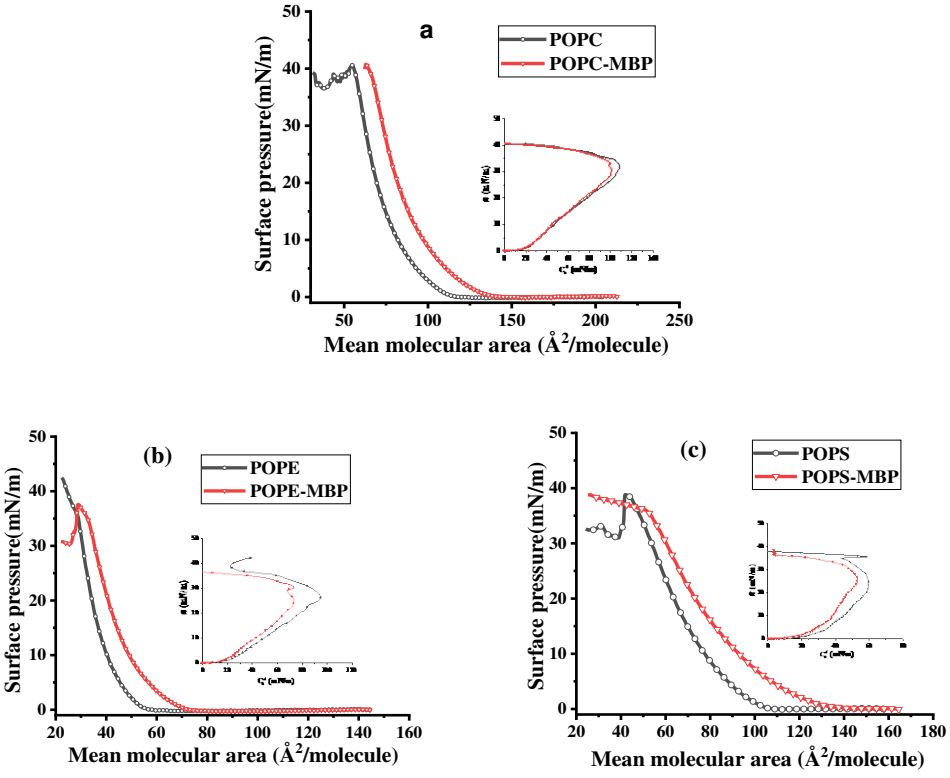

**Fig.2** Compression isotherms and π- $C_s^{-1}$(insert) of POPC (a), POPE (b), and POPS(c) on 1nM MBP subphase**.**

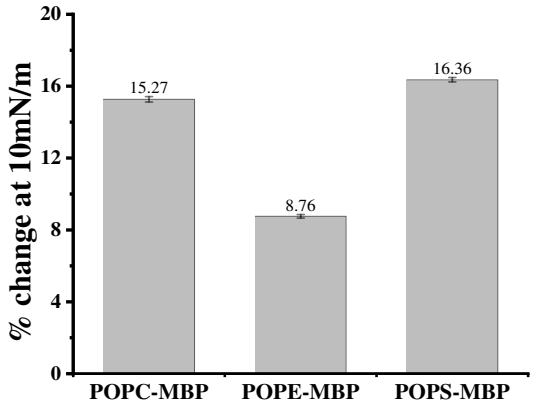


**Fig.3** The mean molecular area (MMA) change in % at a surface pressure of 10 mN/m upon mixing the MBP with the different head group of phospholipids.

**Table 1**

Mean molecular area (Å$^2$) at lift-off, π=10 mN/m, collapse and % change along with the compressibility moduli ( $C_s^{-1}$) with MBP ($C_{MBP}$=1.0 nM) for POPC, POPE and POPS.

| **Lipid-MBP** | **Mean molecular area (Å$^2$)** | | **Relative change in % (Å$^2$)** | $C_s^{-1}$ **(mN/m)** |
|---|---|---|---|---|
| **(1.0 nM)** | **Lift-off** | **Collapse** | | |
| **POPC** | 117.2 | 54.8 | | 108.5 |
| **POPC/MBP** | 140.0 | 63.0 | 15.3±0.5 | 100.6 |
| **POPE** | 59.4 | 28.7 | | 94.6 |
| **POPE/MBP** | 75.7 | 22.8 | 8.8±0.2 | 73.6 |
| **POPS** | 109.1 | 38.8 | | 59.5 |
| **POPS/MBP** | 133.9 | 26.2 | 16.4±0.3 | 53.1 |

## Two-dimensional virial equation of state for different lipids and MBP interactions

At a low surface pressure (10 mN/m), in order to better explore the characteristics of MBP with phospholipids of different head groups, the π-A curves were analyzed using simple statistical theory (2D-VES). The results of Eq. (2) according to this experiment's parameters are exhibited in Fig.4. The second virial coefficients ($b$ > 0) for these interactions may be explained as the interactions between the heads of the molecules are repulsive. The analysis showed that the inclusion of 1nM MBP into the subphase makes the repulsion coefficient to increase from 0.2624 to 0.3072 (POPC), 0.1322 to 0.1678

(POPE), and 0.2435 to 0.3023 (POPS), respectively, which is consistent with the increase of the lift off area in the existence of MBP. The aggregation coefficient was obtained for the pure POPC, POPE and POPS monolayers at a surface pressure of 10 mN/m. Beyond that, all monolayers show very low aggregation coefficients ($a < 1$), indicating the higher aggregation of intermolecular at a surface pressure of 10 mN/m, which could be due to electrostatic and hydrophobic interactions between the MBP and the three types of phospholipid head groups.

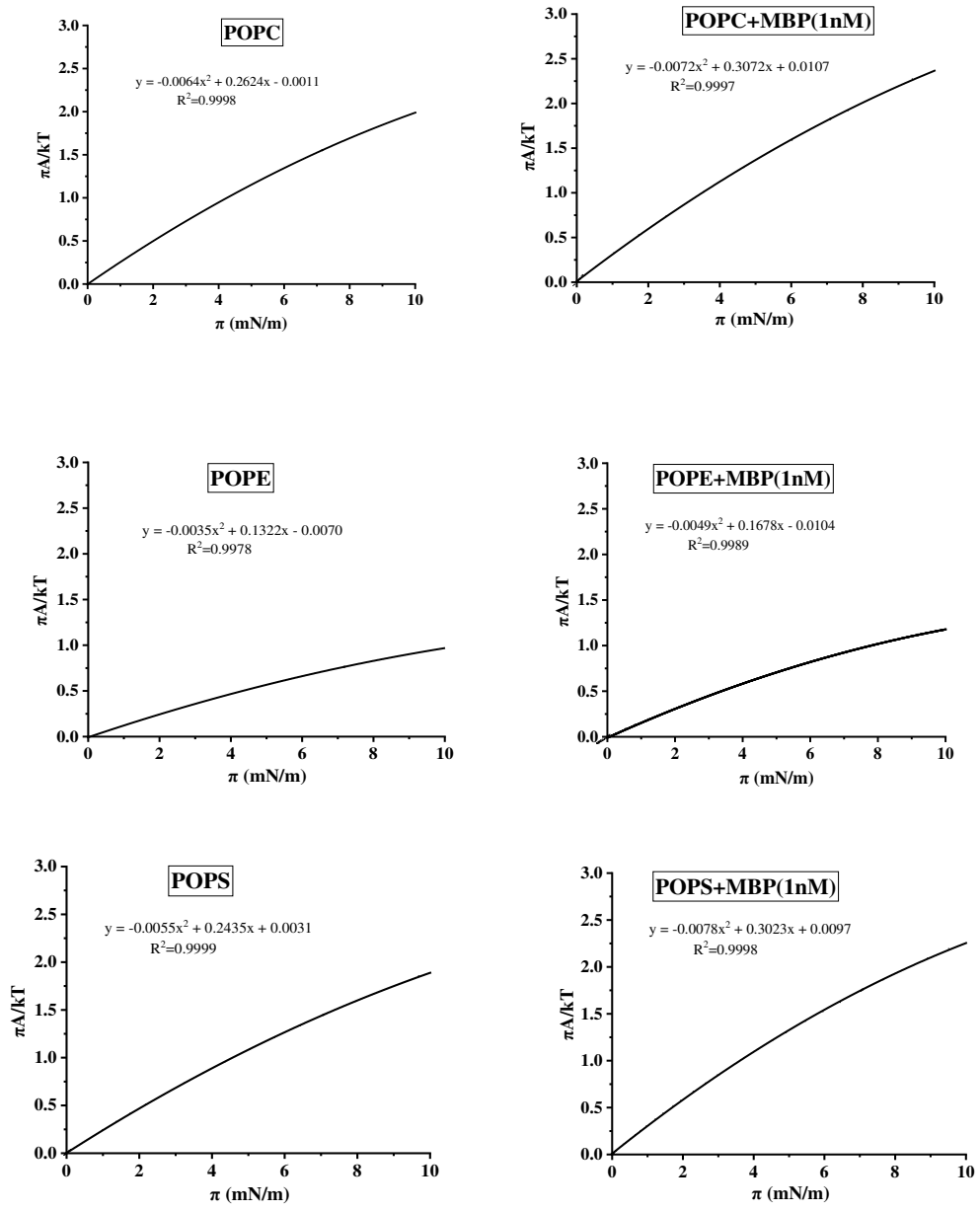


**Fig.4** 2D-VES theoretical study of the pure phosphatides (POPC, POPE, and POPS) and the mixed POPC/MBP, POPE/MBP, and POPS/MBP surface monolayers.

## Morphological monitoring of MBP with the POPC, POPE, and POPS monolayers using AFM

To further evaluate potential microstructure changes within the mixed monolayers upon lipid (POPC, POPE, and POPS)-MBP interaction, AFM was used to characterize the surface topography via contact mode. AFM topographic images were taken from POPC-MBP, POPE-MBP, and POPS-MBP LB films following the adsorption of the Tris-HCl subphase, which was seen to increase the concentration of MBP at 1 nM at $\pi$=10 mN/m. MBP molecules were found to possess granular features (Fig.5), and the cross-sectional lines in the height profile demonstrated that the aggregation of MBP molecules. The height of the pure phospholipid monolayer is about 2 nm. The measured protein has a diameter of 30~120 nm and a height of 6~32 nm. This value is much higher than the phospholipid monolayer. Therefore, the white spherical particles we observed are aggregates of proteins. Significant changes occurred in the Tris-HCl subphase containing MBP at constant concentration. The images seen in Fig.6 show the monolayers' heterogeneity induced by the presence of MBP. At a surface pressure of 10 mN/m, the monolayers of POPC, POPE, and POPS were observed to be stable until the addition of MBP. However, when MBP with a concentration of 1 nM in the subphase, the quantity of MBP particle domains as well as topographical changes observed at 10 mN/m become increasingly obvious. This phenomenon indicated that MBP molecules are embed into the lipid monolayer, making the mean molecular area larger. These results are consistent with similar $\pi$-A isotherms and the second virial coefficients shown in Fig.2 and Fig.4, which are also due to the strong interactive effects of MBP to POPC, POPE, and POPS, resulting in a high compaction of myelin sheath. Regarding the MBP-POPE monolayer, it appeared that the participation of MBP did not induce the obvious morphological changes on the monolayer as seen in Fig.6 (c, d), the adsorbed amount of MBP was greatly increased by with a rise in the concentration of MBP. From the MBP concentrations in the subphase of the 1 nM image, more "collapse domain" was formed on the POPC monolayer (Fig.6b and Fig.7a) with a height of 0.44~3.88 nm, indicating that MBP molecules were squeezed into the subphase because of interactions. In terms of the mixed monolayer systems featuring MBP-POPS, the presence of MBP induced significant changes in organizational structure, which is especially evident at concentrations at 1nM. In addition, the domain structures changes from "disk-like" to "densely-branched" structures observed on the Tris-HCl subphase (Fig.6(e,f)). Moreover, numerous MBP particles were adsorbed on the surface of the POPE and POPS monolayers, various aggregated protein particles with diameters up to 0.3 μm as well as relative heights of 9.2 nm (MBP-POPE) and 6.5 nm (MBP-POPS) were evident and depended on the lipid surface roughness, as seen in Fig.7(b, c). These results are in accordance with the previous analysis of the second virial coefficients, which further illustrates that MBP-lipid (POPC, POPE, and POPS) interactions show a significant dependence on concentration and is likely

governed by electrostatic and hydrophobic forces. Such interactions are further illustrated by the model in Fig.8.

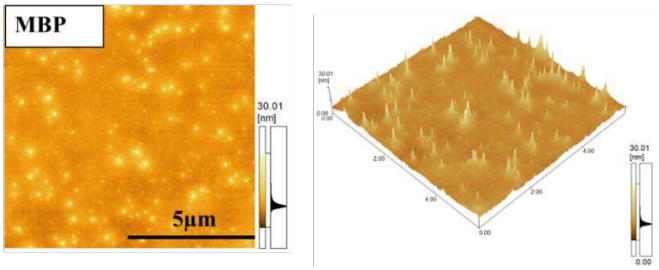


**Fig.5** AFM images (10μm×10μm) of LB films transferred at 10mN/m for MBP. Scale bar=5μm.

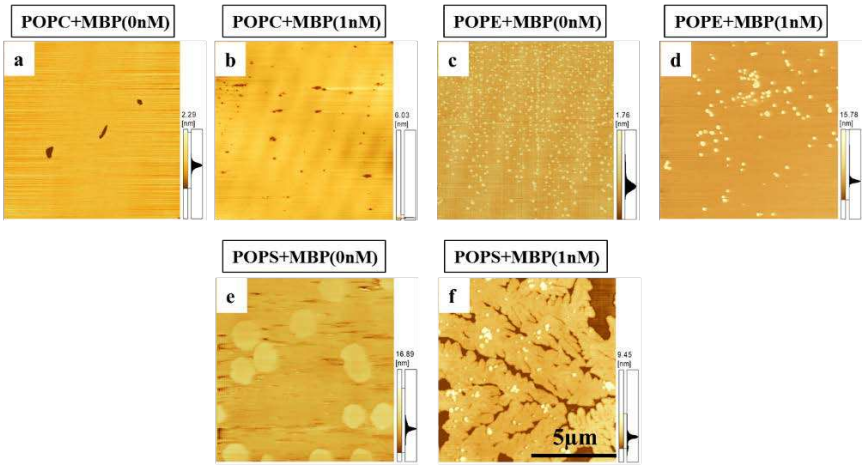


**Fig.6** AFM micrographs of the phospholipid monolayer with different head groups (POPC, POPE, and POPS) at a constant surface pressure (10mN/m) on the Tris-HCl subphase with $C_{MBP}$=0nM and 1nM at 295.2K. The scale bars in the lower-right are equal to 5μm.

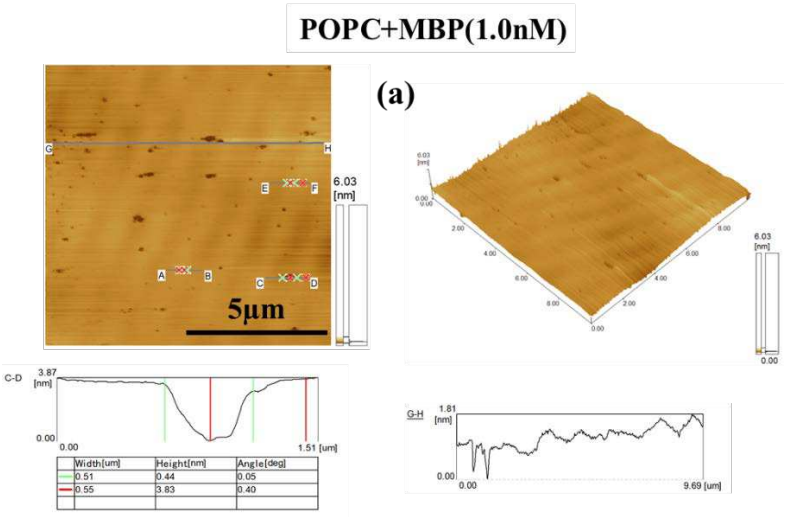

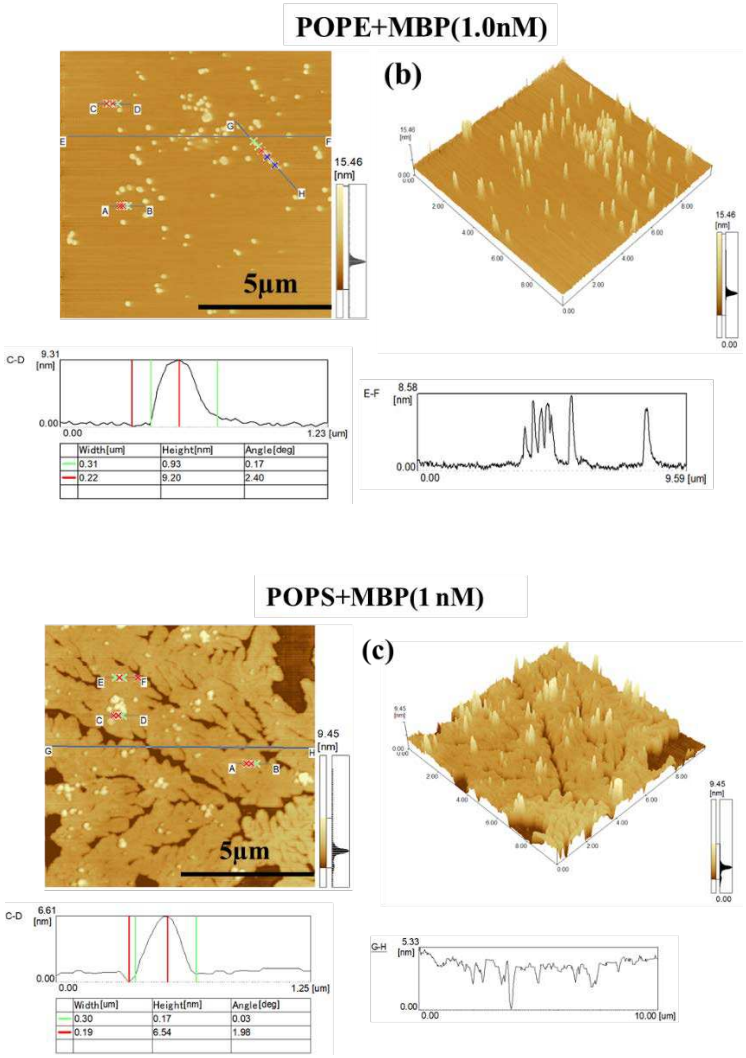


**Fig.7** AFM topographic mixed monolayers (MBP-POPC, MBP-POPE, and MBP-POPS) transferred on mica at 10 mN/m from the subphase at constant concentrations of MBP. (a) POPC +MBP(1nM), (b) POPE +MBP(1nM) and (c) POPS + MBP(1nM). Cross-sectional analysis based on the horizontal line shown. The scan size and height scale are given for each image. Scale bar = 5 µm.

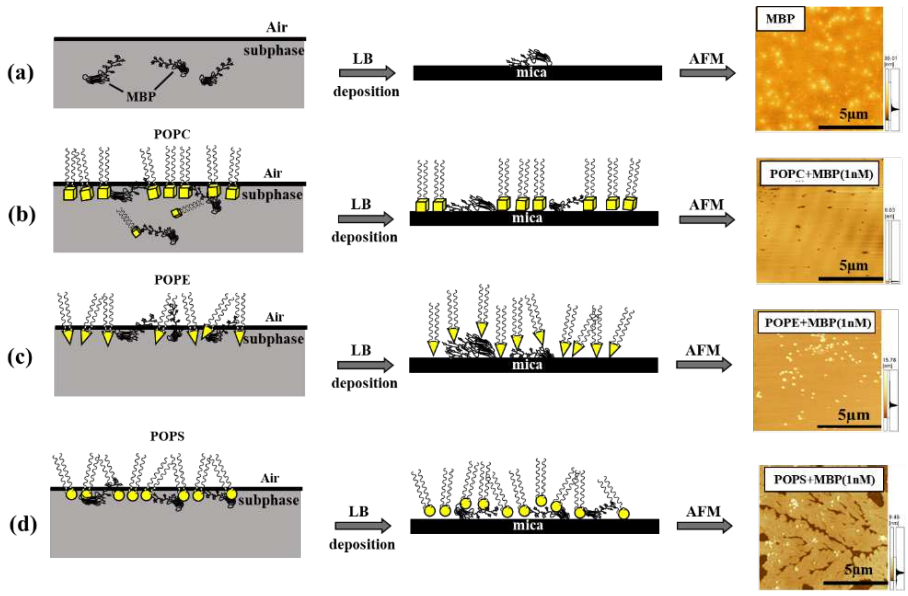


**Fig.8** Schematic presenting the model of pure MBP in Tris-HCl subphase (a) and interaction with POPC+MBP (1.0 nM) (b), POPE+MBP (1.0 nM) (c), and POPS+MBP (1.0 nM) (d) at constant concentration.

## Conclusions

In conclusion, this study demonstrates the analysis of the monolayers' characteristics, compressibility, and conformational changes on LB films for MBP and the major myelin lipid (POPC, POPE, and POPS). Here, MBP-lipid monolayer interactions are not only governed by electrostatic interactions (MBP-POPS), and this study focuses on the role of hydrophobic interactions at the concentration MBP of 1nM during insertion and adsorption into neutral lipids (MBP-POPC and MBP-POPE), where electrostatic attractions were observed between positively charged MBP and negatively charged polar head POPS lipids, prompting the adsorption of MBP. (1) The quantitative and qualitative analyses of second virial coefficients as well as the compressibility modulus ( $C_s^{-1}$ ) for these interactions demonstrate an increase in the area per molecule at the MBP concentration of 1nM for mixed monolayers as well as the formation of a highly ordered and stable pure lipid monolayer. (2) The presence of MBP induced conformational changes in the monolayer when mixed with three lipids. When mixed with POPE+MBP and POPS+MBP, the MBP particles were adsorbed into the monolayer. In terms of POPC, its molecules were squeezed into the subphase. (3) These findings may provide qualitative and quantitative information on MBP adsorption mechanisms for major myelin lipids (POPC, POPE, and POPS), which maintain the tightly packed multilamellar structure of the myelin sheath by hydrophobic and electrostatic interactions.

The results of our study to rise the questions about interactions of MBP with other lipid models, such as "lipid raft", "plasma membrane", and "myelin membrane model". The myelin lipid bilayers had a lipid conformational characteristic of myelin from "healthy" and "disease-like" in the

cytoplasmic leaflets. They exhibit different adsorption mechanisms. We will study the relevant issues in this field in due course.

## Conflict of interest

The authors declare that they have no confict of interest.

## References


1. Selek, S., Esrefoglu, M., Meral, I., Bulut, H. & Bayindir, N. Effects of Oenothera biennis L. and Hypericum perforatum L. extracts on some central nervous system myelin proteins, brain histopathology and oxidative stress in mice with experimental autoimmune encephalomyelitis. *Biotech. Histochem.* **94**, 75-83 (2019).
2. Tsuge, H. A myelin sheath protein forming its lattice. *J. Biol. Chem.* **295,** 8706-8707 (2020).
3. Harauz, G.& Musse, A. A. A Tale of Two Citrullines—Structural and Functional Aspects of Myelin Basic Protein Deimination in Health and Disease. *Neurochem. Res.* **32**, 137-158 (2007).
4. Widder, K., Träger, J., Kerth, A., Harauz, G. & Hinderberger, D. Interaction of myelin basic protein with myelin-like lipid monolayers at the air-water interface. *Langmuir*. **34,** 6095-6108 (2018).
5. Matthieu, J. M., Reigner, J., Costantino-Ceccarini, E., Bourre, J. M. & Rutti, M. Abnormal sulfate metabolism in a hereditary demyelinating neuropathy. *Brain Res.* **200**, 457-465 (1980).
6. Dupouey, P., Jacque, C. & Bourre, J. M. Immunochemical studies of myelin basic protein in shiverer mouse devoid of major dense line of myelin. *Neurosci. Lett.* **12**, 113-118 (1979).
7. Arroyo, E. J. & Scherer, S. S. On the molecular architecture of myelinated fibers. Histochem. *Cell Biol.***113**, 1-18 (2000).
8. Krämer, E. M., Schardt, A. & Nave, K. A. Membrane traffic in myelinating oligodendrocytes. *Microsc. Res. Techniq.* **52**, 656-671 (2010).
9. Nicole, B. & Danielle, P. D. Biology of Oligodendrocyte and Myelin in the Mammalian Central Nervous System. *Physiol. Rev.* **81**, 871-927(2001).
10. Zhang, L., Hao, C. C., Wu, S. J., Lu, X. L., Li, J. H. & Sun, R. G. A thermodynamic analysis of the effects of myelin basic protein (MBP) on DPPS and DPPG monolayers. *Colloid Surface A.* **511**, 303-311 (2016).
11. Zhang, L., Hao, C. C., Feng, Y., Gao, F., Lu, X.L., Li, J. H. & Sun, R. G. Analysis of the induction of the myelin basic protein binding to the plasma membrane phospholipid monolayer. *Chinese Phys. B.* **25**, 090507 (2016).
12. Zhang, L., Hao, C. C., Xu, G. Q. & Sun, R. G. Effects of Concentration and Surface Pressure on MBP Interaction with Cholesterol in Langmuir Films. *Scanning*. **2017**, 1-9 (2017).
13. Rispoli, P., Carzino, R., Svaldo-Lanero, T., Relini, A., Cavalleri, O., Fasano, A., Liuzzi, G. M., Carlone, G., Riccio, P., Gliozzi, A. & Rolandi, R. A Thermodynamic and Structural Study of Myelin Basic Protein in Lipid Membrane Models. *Biophys. J.* **93**, 1999-2010 (2007).
14. Polverini, E., Arisi, S., Cavatorta, P., Berzina, T., Cristofolini, L., Fasano, A., Riccio, P. & Fontana,

M. P. Interaction of Myelin Basic Protein with Phospholipid Monolayers:? Mechanism of Protein Penetration. *Langmuir.* **19**, 872-877 (2003).

15. Cristofolini, L., Fontana, M. P., Serra, F., Fasano, A., Riccio, P. & Konovalov, O. Microstructural analysis of the effects of incorporation of myelin basic protein in phospholipid layers. *Eur. Biophys. J.* **34**, 1041-1048 (2005).
16. Haas, H., Steitz, R., Fasano, A., Liuzzi, G. M., Polverini, E., Cavatorta, P. & Riccio, P. Laminar Order within Langmuir-Blodgett Multilayers from Phospholipid and Myelin Basic Protein: A Neutron Reflectivity Study. *Langmuir*. **23**, 8491-8496 (2007).
17. Knoll, W., Peters, J., Kursula, P., Gerelli, Y., Ollivier, J., Deme, B., Telling, M., Kemner, E. & Natali, F. Structural and dynamical properties of reconstituted myelin sheaths in the presence of myelin proteins MBP and P2 studied by neutron scattering. *Soft Matter*. **10**, 519-529 (2014).
18. Maggio, B. & Cumar, F. A. Antigen-dependent alterations in lipid composition of the CNS in guinea pigs with experimental allergic encephalomyelitis," *Brain Res.* **77**, 297-307(1974).
19. Sabatini, K., Mattila, J. P. Kinnunen, P. K. J. Interfacial Behavior of Cholesterol, Ergosterol, and Lanosterol in Mixtures with DPPC and DMPC. *Biophys. J.* **95**, 2340-2355 (2008).
20. Mladenova, K., Petrova, S. D., Georgiev, G. A., Doumanova, V. M. & Lalchev, Z. Interaction of Bestrophin-1 with 1-palmitoyl-2-oleoyl-sn-glycero-3-phosphocholine (POPC) in surface films. *Colloid Surface B.* **122**, 432-438 (2014).
21. Faye, N. R., Moroté, F., Heywang, C. G. & Bouhacina, T. C. Oxidation of Langmuir-Blodgett films of monounsaturated lipids studied by atomic force microscopy. *Int. J. Nanotechnol.* **10**, 390-403 (2013).
22. Mirheydari, M., Mann, E. K. & Kooijman, E. E. Interaction of a model apolipoprotein, apoLp-III, with an oil-phospholipid interface. *Biochim. Biophys. Acta.* **2018**, 396-406 (2018).
23. Garcia-Manyes, S., òscar Domènech., Sanz, F., Montero, M. T. & Hernandez-Borrell, J. Atomic force microscopy and force spectroscopy study of Langmuir-Blodgett films formed by heteroacid phospholipids of biological interest. *Biochim. Biophys. Acta.* **1768**, 0-1198 (2007).
24. Rey Gómez-Serranillos, I., MinOnes, J., Dynarowicz-LaTka, P. & Conde, O. Surface Behavior of Oleoyl Palmitoyl Phosphatidyl Ethanolamine (OPPE) and the Characteristics of Mixed OPPE Miltefosine Monolayers. *Langmuir*. **20**, 11414-11421 (2004).
25. Steinkopf, S., Hanekam, L., Schaathun, M., Budnjo, A., Haug, B. E. & Nerdal, W. Interaction of local anaesthetic articaine enantiomers with brain lipids: A Langmuir monolayer study. *Eur. J. Pharm. Sci.* **47**, 394-401 (2012).

## Acknowledgements

The work was supported by the Special Scientific Research Program supported by Shaanxi Education Department (No. 19JK0429).

## Author contributions

Lei Zhang wrote the main manuscript text and Ming Zhang and Runguang Sun prepared figures 2,3,7.

All authors reviewed the manuscript.

# Figures

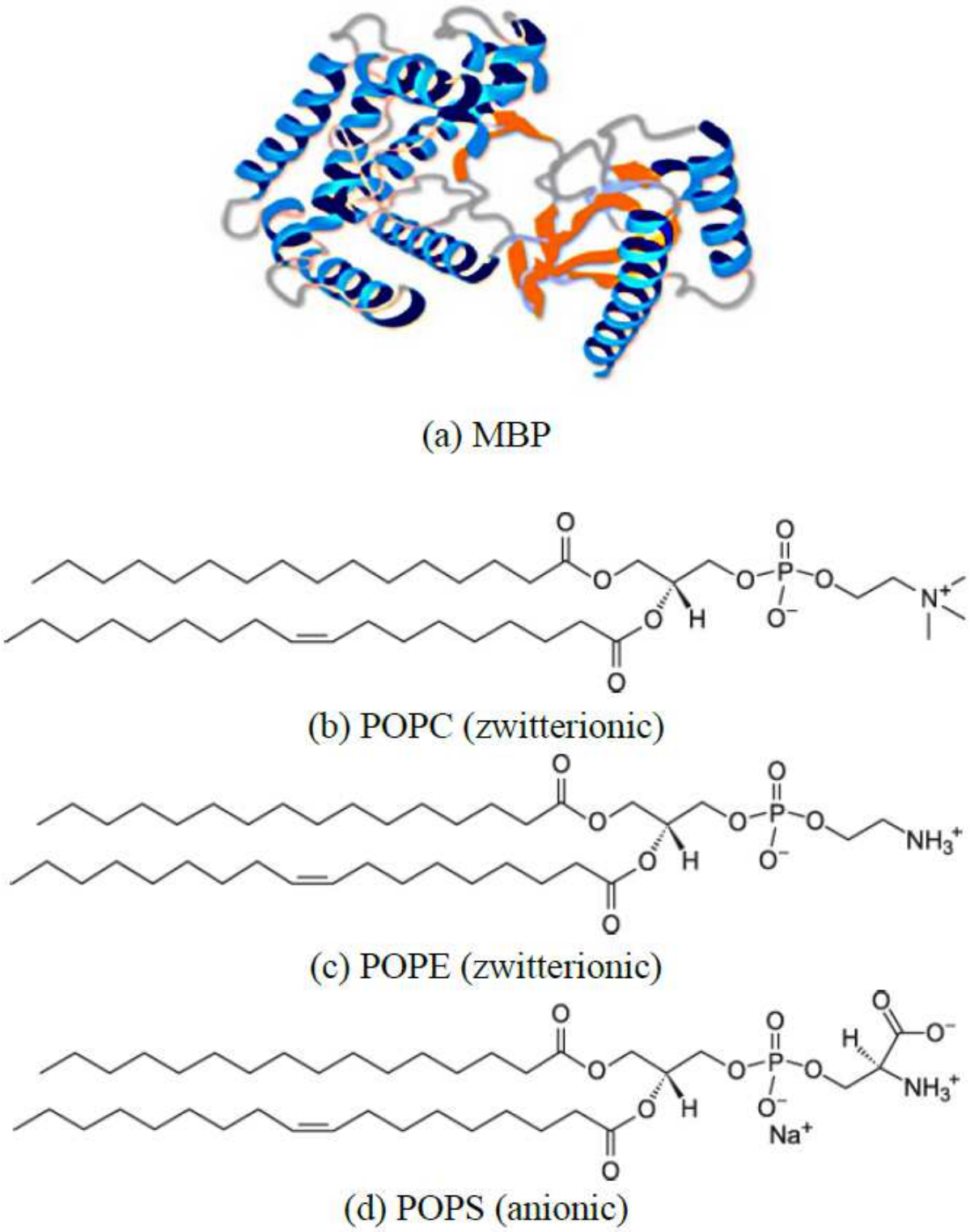


**Figure 1**

The chemical structure of (a) MBP, (b) POPC, (c) POPE, and (d) POPS

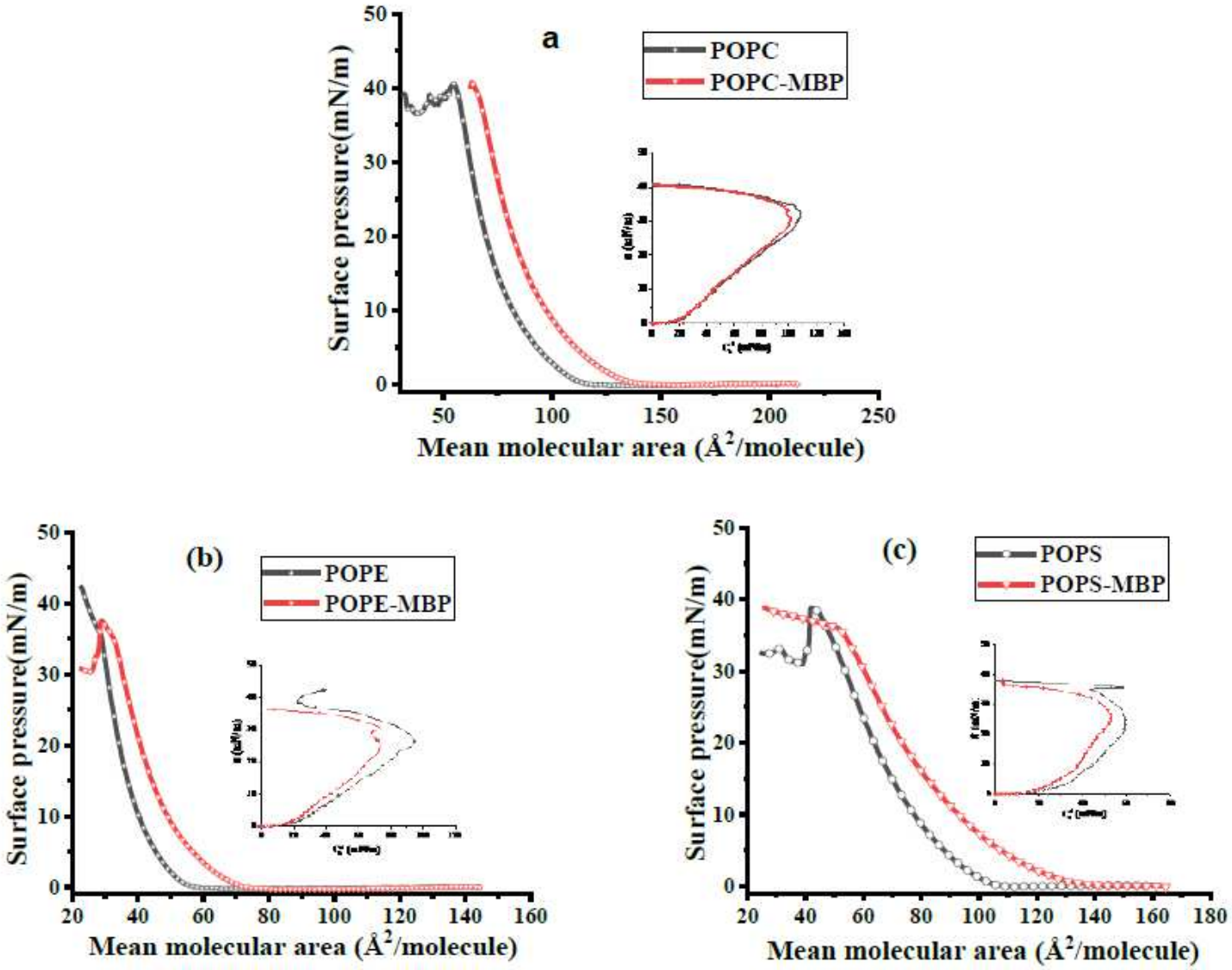


## Figure 2

Compression isotherms and π C−1s (insert) of POPC (a), POPE (b), and POPS(c) on 1nM MBP subphase.

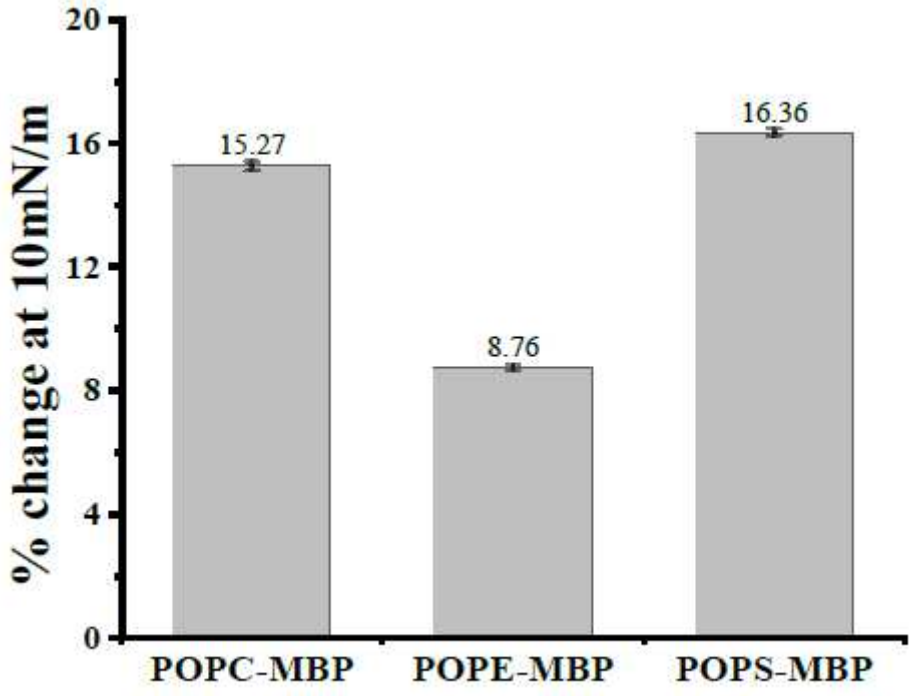


**Figure 3**

The mean molecular area (MMA) change in % at a surface pressure of 10 mN/m upon mixing the MBP with the different head group of phospholipids.

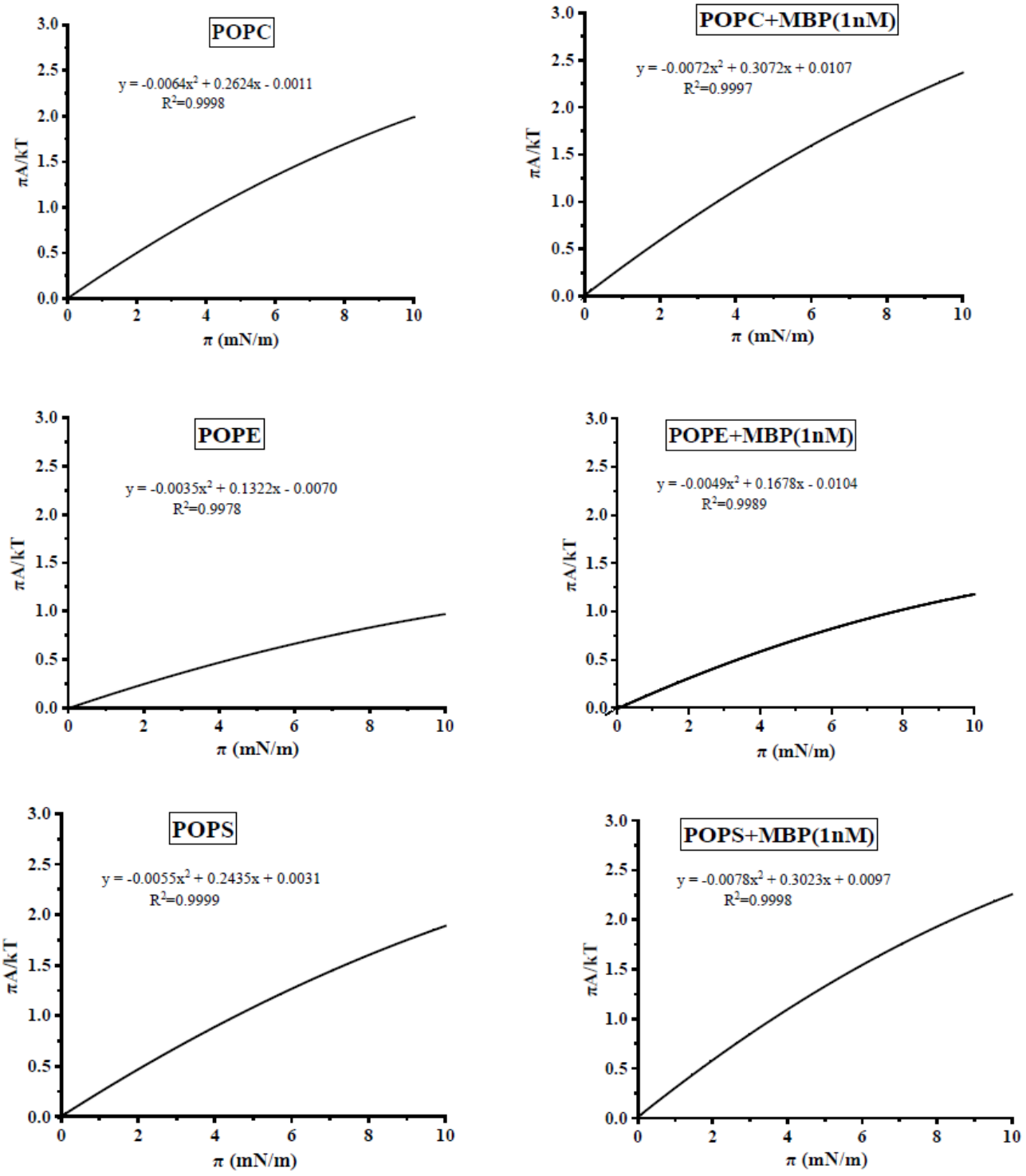


## Figure 4

2D-VES theoretical study of the pure phosphatides (POPC, POPE, and POPS) and the mixed POPC/MBP, POPE/MBP, and POPS/MBP surface monolayers.

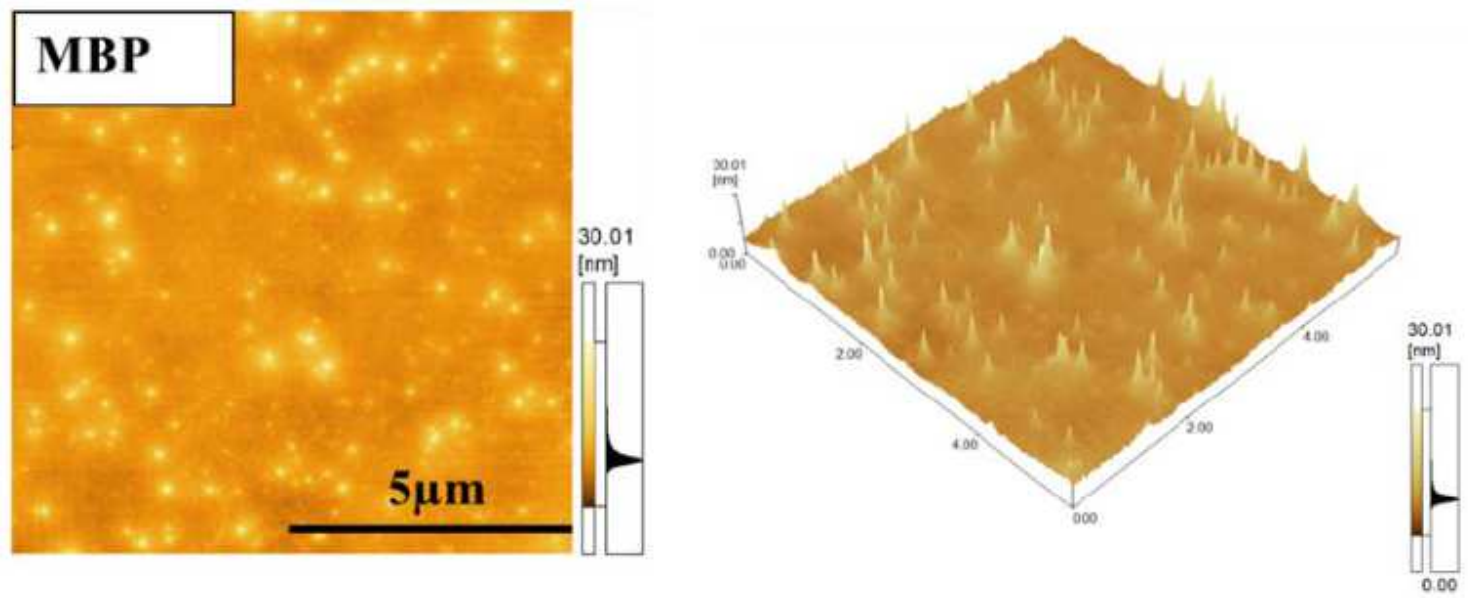


**Figure 5**

AFM images (10μm×10μm) of LB films transferred at 10mN/m for MBP. Scale bar=5μm.

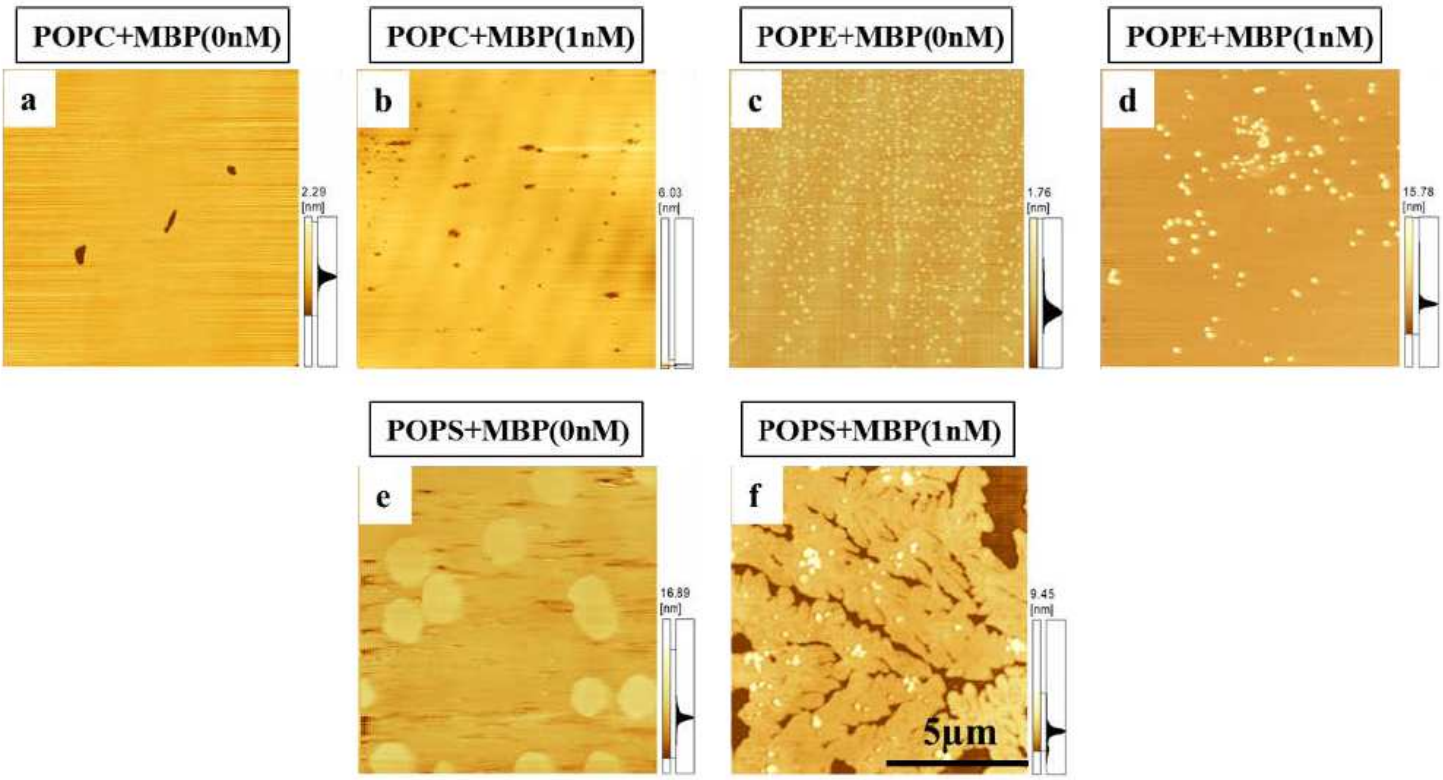


**Figure 6**

AFM micrographs of the phospholipid monolayer with different head groups (POPC, POPE, and POPS) at a constant surface pressure (10mN/m) on the Tris-HCl subphase with CMBP=0nM and 1nM at 295.2K. The scale bars in the lower-right are equal to 5μm.

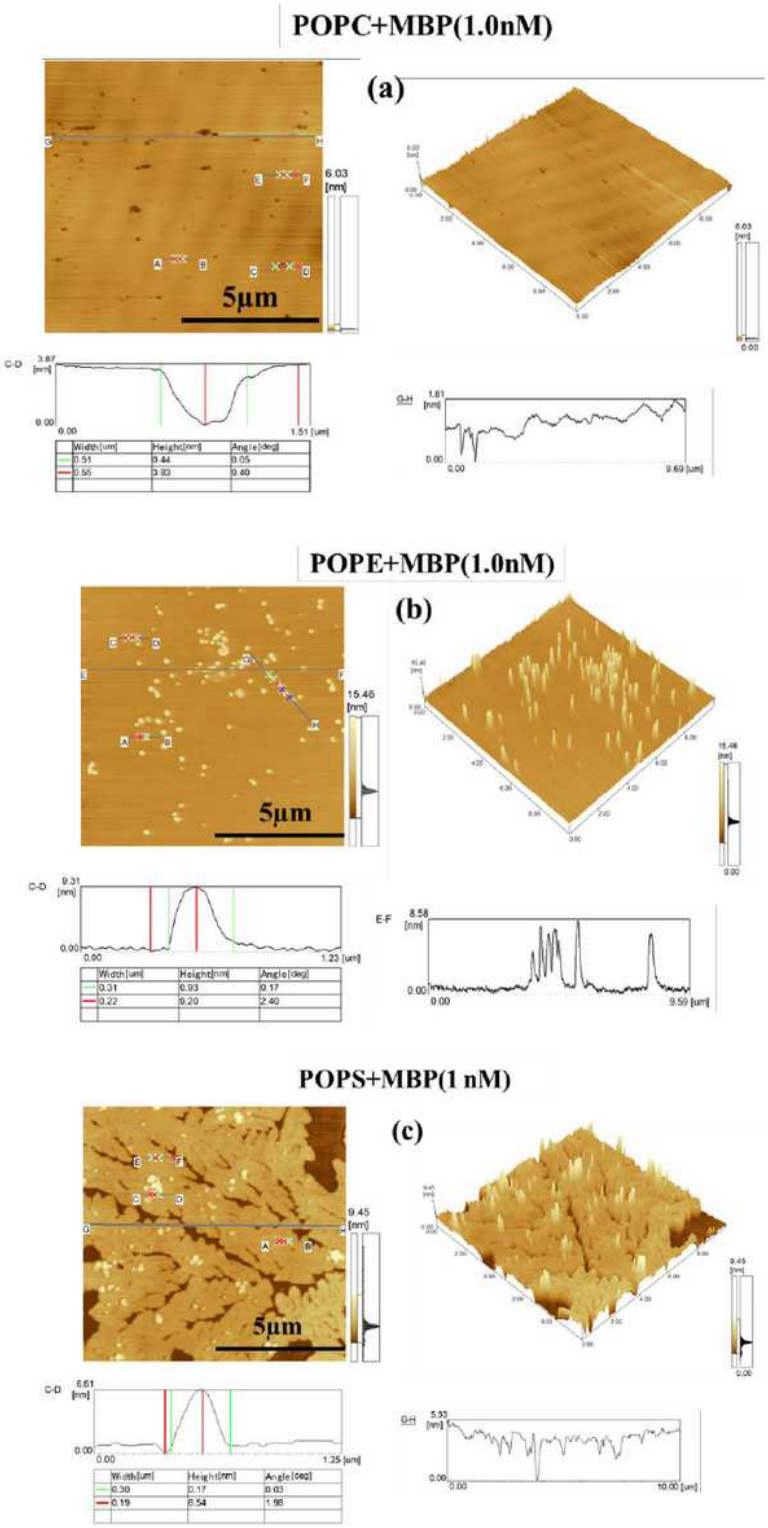


## Figure 7

AFM topographic mixed monolayers (MBP-POPC, MBP-POPE, and MBP-POPS) transferred on mica at 10 mN/m from the subphase at constant concentrations of MBP. (a) POPC +MBP(1nM), (b) POPE +MBP(1nM) and (c) POPS + MBP(1nM). Cross-sectional analysis based on the horizontal line shown. The scan size and height scale are given for each image. Scale bar = 5 µm.

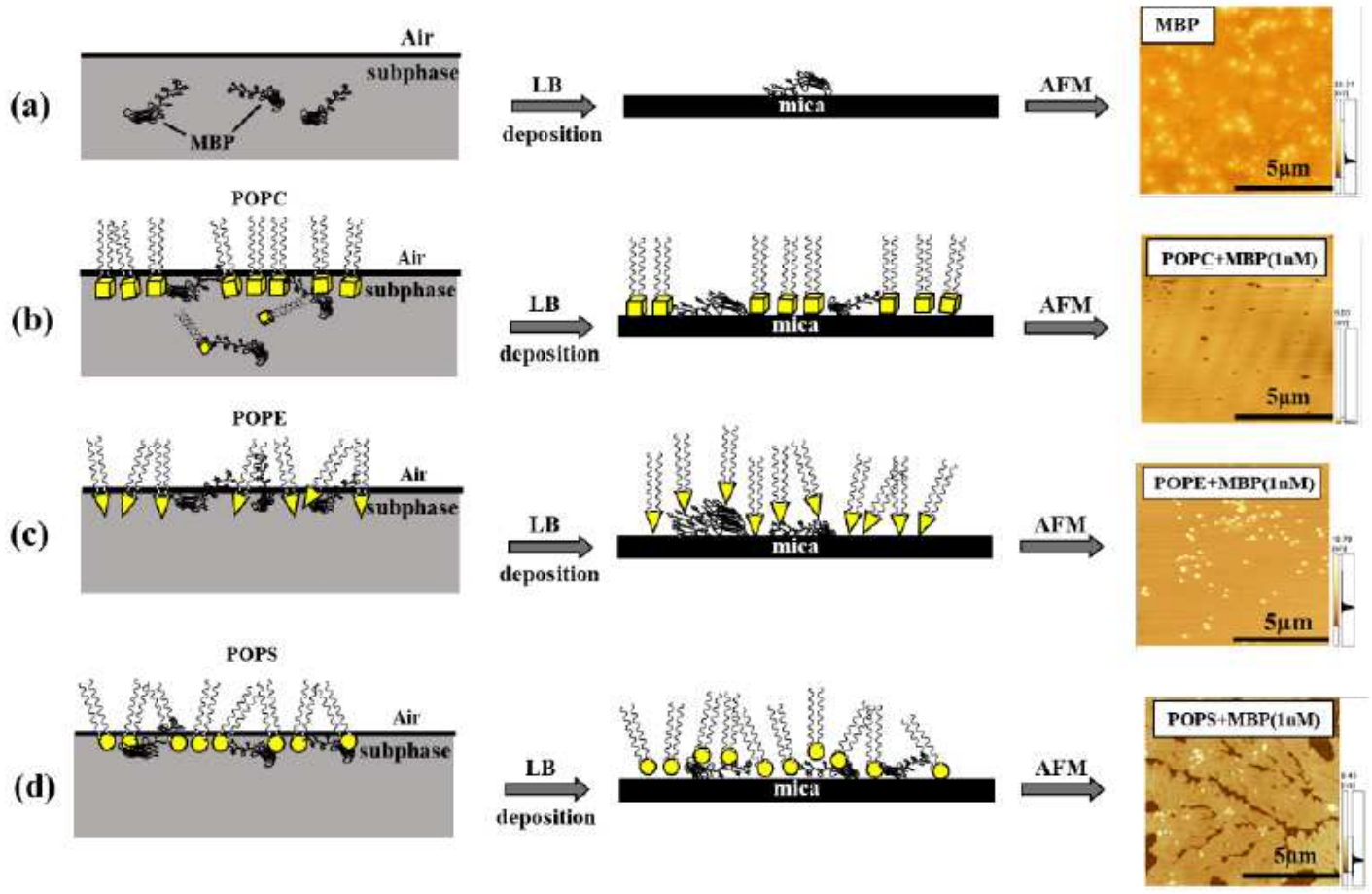


## Figure 8

Schematic presenting the model of pure MBP in Tris-HCl subphase (a) and interaction with POPC+MBP (1.0 nM) (b), POPE+MBP (1.0 nM) (c), and POPS+MBP (1.0 nM) (d) at constant concentration.